Effect of Elevated Temperature on Microstructure and Mechanical Properties of Hot-Rolled Steel

Ali Malik Saadoon
Department of Aeronautical Engineering, University of Baghdad, Baghdad 10071, Iraq
alimsaadun@uobaghdad.edu.iq

Mohanned Al Gharawi
Department of Civil Engineering, University of Baghdad, Baghdad 10071, Iraq
mohanned.algharawi@coeng.uobaghdad.edu.iq

Alaa Al-Mosawe
Department of Civil Engineering, University of Baghdad, Baghdad 10071, Iraq | Swinburne University of Technology, VIC 3122, Australia
aalmosawe@coeng.uobaghdad.edu.iq (corresponding author)

Received: 26 September 2024 | Revised: 13 October 2024 and 20 October 2024 | Accepted: 21 October 2024

 DOI: https://doi.org/10.48084/etasr.9108

ABSTRACT

The mechanical properties and microstructure of hot-rolled steel are critical in determining its performance in industrial applications, particularly when exposed to elevated temperatures. This study examines the effects of varying temperatures and soaking times on these properties through a series of controlled experiments. The primary objective was to optimize the key response parameters, including tensile strength, yield strength, and elongation, by analyzing the influence of temperature and time. A full factorial design approach was used, applying the desirability function theory to explore all possible combinations and identify optimal processing conditions. The experimental results showed that the soaking time played a critical role, significantly influencing the mechanical properties with an impact ratio of 62%. The microstructural analysis displayed that higher temperatures and longer soaking times resulted in the formation of coarser ferrite and pearlite grains, contributing to a decrease in strength and an increase in ductility. The optimum process condition - 650 °C for 60 min - produced the highest values for tensile strength (400.32 MPa), elongation (36.78%) and yield strength (288.52 MPa). The study also highlighted the temperature-dependent nature of the mechanical behavior of hot-rolled steel. While tensile strength and yield strength initially increase with temperature, prolonged exposure, particularly at 600 °C and 750 °C, results in significant grain coarsening and a corresponding degradation of these properties. Conversely, elongation improves at moderate temperatures (150 °C to 300 °C) but decreases with prolonged exposure, especially at higher temperatures. These findings underscore the importance of precise control of thermal processing parameters to optimize the mechanical properties of hot-rolled steel. The findings offer significant insights that can be leveraged to optimize material performance in industrial applications, where thermal exposure is a critical consideration.

Keywords-hot-rolled steel; mechanical properties; microstructure evaluation; desirability function; soaking time

I. INTRODUCTION

The mechanical properties and microstructure of hot-rolled steel are of critical importance in the assessment of the structural integrity of steel members subjected to fire or elevated temperatures. These conditions induce substantial alterations in the material's microstructure and phase due to the varying heating and cooling rates. Nevertheless, a comprehensive understanding of steel behavior under such circumstances remains a challenging problem, particularly in terms of accurately replicating elevated temperature exposure in controlled experimental settings [1]. A substantial body of research has been dedicated to the analysis of the mechanical properties and microstructure of steel grades utilized in the manufacturing of aircraft and automotive components [1, 2]. Steel, which is an alloy primarily composed of iron with a carbon content ranging from 0.2% to 2.1% by weight, has recently received considerable attention in the context of High-Strength Steel (HSS) and Very High-Strength Steel (VHSS). The introduction of alloying elements, including manganese, chromium, vanadium, and specific semiconductors, can significantly improve the mechanical properties of steel when incorporated in precise proportions. These alloying additions enhance the material's hardness, plasticity, and durability [3]. Furthermore, advancements in heat treatment methodologies, such as post-hot forming tempering processes, have increased the ductility of hot-rolled steel sheets [4]. Furthermore, experimental studies have demonstrated that Advanced High-Strength Steel (AHSS) exhibits a favorable balance between high strength and ductility when subjected to warm working conditions. Tensile tests conducted at temperatures spanning from 20 °C to 700 °C during High-Temperature Thermomechanical Treatments (HTMT) have demonstrated that yield strength tends to increase within this temperature range, offering a potential advantage over traditional heat treatment methods [5]. The distinction between the effects of elevated temperatures and heat treatments lies in the different approaches employed to alter the chemical and physical properties of metals. The process of elevated temperature exposure involves heating or cooling metals from a solid state to extreme temperatures, followed by a controlled cooling process that is intended to modify the microstructure and, as a consequence, the material properties [3]. It is imperative to possess a comprehensive understanding of heat treatment methods, as they facilitate the imparting of specific properties to metals [6, 7]. The primary objective of heat treatment in steel is to regulate the combination of phases by adjusting heating conditions and selecting appropriate cooling conditions to obtain the desired properties based on the requirements of the intended application [8, 9]. The preceding studies concentrate on the mechanical properties of steel when subjected to a specific temperature range over a defined soaking period. However, in actual fire incidents, steel structures are subjected to fire until the fire is extinguished. The present study examined the impact of fire exposure duration on steel specimens, while also considering the influence of varying temperature levels. The response parameters, including ultimate tensile strength, yield strength, elongation, and the microstructure of hot-rolled steel, were analyzed using the desirability function approach with a full factorial design to ascertain the optimal conditions. The use of hot-rolled steel in a variety of industrial applications has been the subject of extensive study.

II. MATERIALS AND TESTING METHOD

A. Materials

The metal used in this study is a commercial-grade hot-rolled steel, with properties that align with the ISO 4995-HR 235 specification limits [27]. The chemical composition and mechanical properties of this steel are presented in Tables I and II, respectively.

B. Testing Method

1) Specimen Properties

Tensile test samples were prepared in accordance with the specifications set forth in ISO 6892-1 [28, 29]. The gauge lengths and areas of the tensile test samples were recorded prior to loading, as shown in Figure 1. The standard specimens were prepared in accordance with the capabilities and specifications of the testing apparatus.

TABLE I. CHEMICAL COMPOSITION OF STEEL

Element	**%**	**Element %**	**%**
C	0.141	V	0.0017
Si	0.0082	W	0.005
Mn	0.427	Pb	0.001
P	0.0005	Sn	0.001
S	0.001	Zr	0.0025
Cr	0.0069	Zn	0.0006
Mo	0.001	Cu	0.0045
Ni	0.001	Al	0.028
Sb	0.0083	Fe	Remaining

TABLE II. MECHANICAL PROPERTIES OF STEEL

	Yield (MPa), Reh	**Tensile (MPa), Rm**	**Elongation (%)**
As received	254	390	30.1

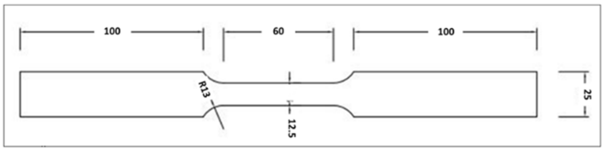

Fig. 1. The standard dimensions of the tested specimens (mm).

2) Testing Method

Tensile tests were conducted using a universal testing machine to investigate the mechanical properties of the steel at room temperature. In the course of these tests, the specimens were subjected to controlled tension until failure. The data obtained from the tensile tests, including the ultimate tensile strength (R_m), yield strength (R_{eh}), and maximum elongation ($_E$), were recorded in accordance with the experimental design outlined in Table II. The samples were heated to the requisite temperatures in a muffle furnace, as depicted in Figure 2. The furnace is capable of reaching a maximum temperature of 1200 °C. In accordance with the full factorial experimental design, two process parameters, each with five levels (5^n, where n is the number of parameters), were evaluated at various temperatures and durations, as detailed in Table III. The heating process was conducted at temperatures ranging from 150 °C to 750 °C, with increments of 150 °C.

TABLE III. THE PROCESS PARAMETERS AND THEIR LEVELS

Process Parameters	**Levels**				
Number	1	2	3	4	5
Temperature (ºC)	150	300	450	600	750
Time (min.)	30	60	90	120	150

III. RESULTS AND DISCUSSION

Over the past decade, researchers have conducted extensive examinations of the effects of elevated temperatures on the mechanical properties and microstructure of hot-rolled steel. Table IV provides a summary of additional research studies in this field, highlighting key findings and methodologies aimed at optimizing these material properties.

TABLE IV. SUMMARY OF PREVIOUS RESEARCH ON HOT-ROLLED STEEL AND RELATED MATERIALS

Item	Ref.	Year	Type of steel	Main observation
1	[10]	2006	Alloy AZ91	Examines elastic-plastic properties of AZ91 magnesium alloy at elevated temperatures. Microstructure was influenced by exploitation conditions, with strength rapidly decreasing above certain temperatures.
2	[11]	2006	Ultrafine grained steels	Ultrafine grain size steels below 1 μm offer a combination of high strength and toughness. Different thermomechanical processes were explored to produce submicron grain structures.
3	[12]	2007	Steel S355, Steel S420M, Steel S460M, Steel S350GD+Z, Steel S355J2H	Extensive study on the mechanical properties of structural steels at elevated temperatures, with comparison to EN1993-1-2 standards. Evaluated design values for structural fire safety.
4	[13]	2009	ASTM A992 Steel	Constitutive models developed for tensile properties, creep, and relaxation at elevated temperatures. Significant gaps in experimental data for predicting the fire response of structural steel.
5	[14]	2009	Mg-Si alloys	Examines the structure and mechanical properties of Mg-Si alloys at elevated temperatures. The study connects microstructure to metallurgical and technological factors influencing properties.
6	[15]	2012	Al-Mg ALLOY	Investigated the mechanical properties of Al-Mg alloys with bimodal grain sizes, showing improved strength at room temperature. Strength decreased rapidly with temperature, with significant grain boundary effects at high temperatures.
7	[16]	2013	Steels containing 9-12% Cr	Investigated microstructural changes in the heat-affected zone (HAZ) of 9–12% Cr steels under simulated welding conditions. Post-weld heat treatment contributed to improved creep resistance at elevated temperatures.
8	[17]	2014	Cr–Cr2 Ta-based alloys	Investigated the influence of Si content on the hardness and yield strength of Cr-Ta-Si alloys at elevated temperatures. High Si content improved yield strength but decreased toughness.
9	[18]	2016	HR3C Steel	Microstructural changes due to Nb and N additions significantly affect the mechanical properties of HR3C steel. Aging at elevated temperatures precipitates compounds like MX, CrNbN, and M23C6.
10	[19]	2017	Low-alloy high-speed steels, HS 6-5-2, HS3-1-2	Hot hardness decreased to 650–700 HV in the 500–550 °C range. Yield stress and hardness remained stable after preheating and testing at room temperature.
11	[20]	2017	Low Carbon Microalloyed Steels	Ultra-fast cooling produced acicular ferrite and granular bainite microstructures with enhanced mechanical properties. Steel B showed superior properties compared to Steel A due to finer grain size and more dispersed precipitates.
12	[21]	2018	Medium carbon steel	Optimal heat treatment parameters include tempering at 400 °C and using TiO2 nanoparticles. Key factors influencing tensile strength and ductility include tempering temperature and type of base media.
13	[22]	2021	High-Mn austenitic steel	Vanadium additions enhance yield strength and suppress recrystallization. High-density dislocations reduce twinning, improving both strength and cryogenic toughness.
14	[23]	2023	Cold-formed steel (CFS)	Elevated temperatures reduce the load-carrying capacity of steel columns, especially above 400 °C. Time-dependent exposure significantly impacts strength loss in CFS columns.
15	[24]	2024	Q355 hot-rolled steel	Mechanical properties at the cooling stage are influenced by peak heating temperature and tensile test temperature. Threshold temperatures for elastic modulus, ultimate strength, and strain are at 600 °C, with the yield strength threshold at 400 °C.
16	[25]	2024	SS317L/ASTM SA516 GR60 Steel	Water quenching leads to an increase in tensile strength from 524 MPa to 652 MPa. Significant changes in mechanical properties are linked to microstructural alterations in the GR60 layer.
17	[27]	2024	Hot-rolled steel bars subjected to corrosion-temperature superimposition	Investigates the combined impact of corrosion and elevated temperatures on hot-rolled steel bars. Identifies the nonlinear relationship between fire exposure and corrosion in structural steel.

Fig. 2. Muffle furnace used for heating the specimens.

The outcomes of the full factorial experimental design, along with the measured response parameters—ultimate tensile strength, yield strength, and elongation—are shown in Tables V to VII and Figures 3 to 5, respectively.

TABLE V. VALUES OF ULTIMATE TENSILE STRENGTH (MPA)

Temp. °C	Time (min.)					
	0	30	60	90	120	150
20	390	390	390	390	390	390
150	390	397	416	413	396	395
300	390	408	405	400	395	400
450	390	401	403	399	386	382
600	390	378	390	375	379	374
750	390	379	371	362	355	355

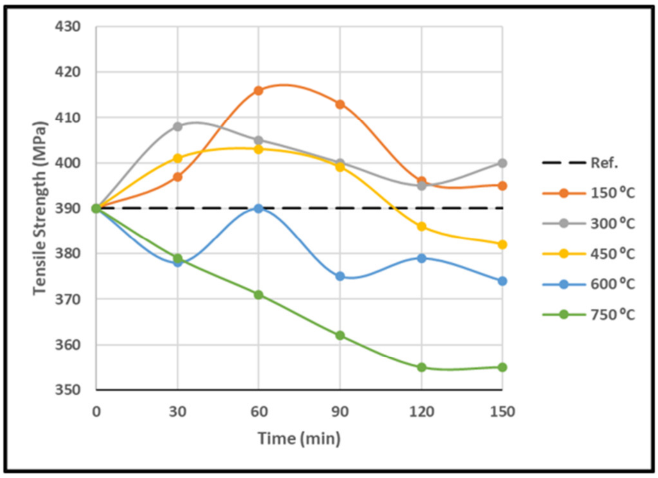

Fig. 3. The response of the ultimate tensile strength (MPa) related with time (min) and temperature (°C).

This segment of the study examines the influence of temperature and time on the mechanical and microstructure properties of hot-rolled steel. At 150 °C, the ultimate tensile strength begins at 390 MPa, attains a maximum of 416 MPa at the 60-min mark, and subsequently declines to 395 MPa at the 150-min point. This suggests that while the initial exposure results in enhanced strength, prolonged exposure causes some degree of softening. Similarly, at 300 °C, the tensile strength reaches 408 MPa after 30 min, before gradually declining to 400 MPa at 150 min. Although the peak strength at 300 °C is lower than at 150°C, the overall strength remains relatively high. At 450 °C, tensile strength increases to 403 MPa at 60 min but drops to 382 MPa at 150 min.

TABLE VI. VALUES OF THE YIELD STRENGTH (MPA), REH

Temp. C	Time (min.)					
	0	30	60	90	120	150
20	254	254	254	254	254	254
150	254	290	286	287	265	253
300	254	296	297	285	283	251
450	254	290	279	275	271	250
600	254	277	272	270	265	249
750	254	269	270	257	255	244

This phenomenon exhibits a pattern analogous to that observed in lower temperatures, but with a more pronounced decline over time. At 600 °C, a gradual decline in tensile strength was observed, reaching 374 MPa by 150 min, indicative of potential material degradation. The most significant decline occurs at 750 °C, where there is a notable reduction in tensile strength, from 390 MPa to 355 MPa, over the course of 150 min. A comparable pattern is observed in the case of yield strength. At 150 °C, there is an initial increase in tensile strength from 259 MPa to a peak of 290 MPa at 30 min after which there is a decline to 253 MPa by/at 150 min. This demonstrates an initial strengthening effect, which is then followed by a decrease with extended exposure. At 300 °C, the yield strength reaches 297 MPa at 90 min but subsequently declines to 251 MPa at 150 min. At 450 °C, a decrease from 290 MPa to 250 MPa is observed after 150 min, indicating that prolonged exposure at this temperature has a detrimental effect on the material. As the temperature increases to 600 °C and 750 °C, the yield strength continues to decrease, reaching a minimum value of 244 MPa after 150 min. This demonstrates a significant deterioration in the material's strength at elevated temperatures. With regard to elongation, the material displays enhanced ductility at 150 °C, reaching a maximum of 35.76% at 60 min before declining to 32.0% at 150 min. These findings indicate that short-term exposure enhances ductility, whereas prolonged exposure has the opposite effect, reducing it. At 300°C, the maximum elongation reached was 37.49% at the 30-mark mark, declining to 33.86% at the 150-min mark. This illustrates an initial improvement in ductility, followed by a decline over time. At 450 °C, the rate of elongation remains relatively stable, ranging from 34.42% to 36.78%. This indicates that the material exhibits better retention of ductility than at lower temperatures. However, at temperatures of 600 °C and 750 °C, there is a fluctuation in elongation before a reduction to 33.18% and 32.24%, respectively, which is indicative of a similar reduction in ductility with extended exposure. These findings demonstrate that both temperature and exposure time exert a significant influence on the mechanical properties of hot-rolled steel. While moderate temperatures enhance tensile strength and yield strength, as well as elongation, extended exposure, particularly at elevated temperatures (600 °C and 750 °C), results in material degradation and a reduction in mechanical properties. This is of great consequence for the comprehension of the behavior of steel structures when subjected to prolonged high-temperature conditions, such as those experienced during a fire.

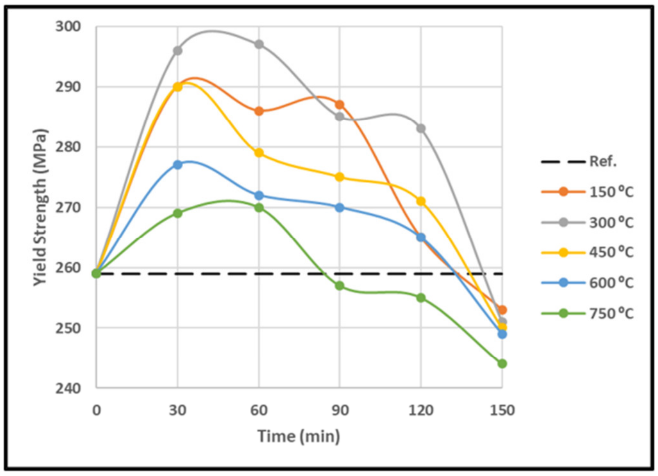

Fig. 4. The response of the yield strength (MPa) related with the time (min) and temperature (°C).

TABLE VII. VALUES OF THE ELONGATION

Temp. °C	Time (min.)					
	0	30	60	90	120	150
20	30.71	30.71	30.71	30.71	30.71	30.71
150	30.71	35.61	35.76	34.42	34.18	32
300	30.71	37.49	37.32	35.4	35.28	33.86
450	30.71	36.74	36.78	36.6	35.77	34.42
600	30.71	35.78	36.34	35.84	35.29	33.18
750	30.71	34.32	35.74	34.37	33.47	32.24

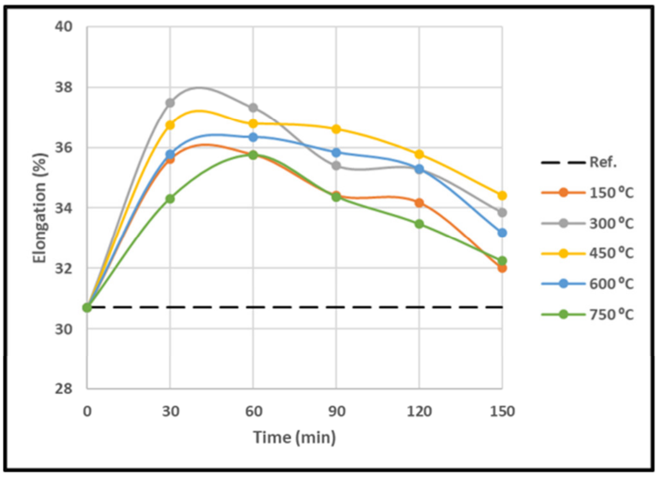

Fig. 5. The response of the elongation related with rime (min.) and temperature (°C).

A. *Microstructural Characterization*

The microstructure of hot-rolled steel is highly sensitive to alterations in temperature and duration of exposure during thermal treatment, as evidenced by the 25 microstructural images presented in Figures 6 and 7. These images document the incremental alterations in the steel's microstructure, which subsequently impact its mechanical properties and overall performance in industrial contexts. The microstructure of the steel remains stable and fine-grained at lower temperatures, approximately 150 °C, as evidenced by images 6 (a), 6 (h), and 6 (i). Despite prolonged exposure of up to 150 min, minimal grain growth occurs, thereby maintaining the uniform distribution of ferrite and pearlite phases. The fine-grained structure contributes to the material's superior tensile strength and toughness, enabling it to withstand mechanical stress effectively. The absence of significant grain growth at these temperatures indicates that the steel can tolerate moderate heating for extended durations without compromising its mechanical properties, which is advantageous for applications requiring both strength and durability. As the temperature increases to the mid-range (300 °C to 450 °C), the interactive effects of temperature and exposure time become increasingly pronounced. As observed in images 6 (k), 6 (n), and 6 (o) at 300 °C, shorter exposure durations (ranging from 30 to 60 min yield a fine, uniform microstructure with minimal grain coarsening. The results demonstrated that when the exposure time was extended to 150 min, there was a notable increase in grain growth, although the overall structural integrity remained relatively stable. Conversely, when the exposure time is increased to 150 min, the growth of grains becomes more pronounced, although the overall structural integrity remains relatively stable. At 450 °C, moderate grain coarsening is observed, particularly with prolonged exposure times (30 to 150 min), as illustrated in images 6 (b), 6 (c) and 6 (m). This grain growth indicates a transition in the material properties of the steel, which is characterized by a gradual decline in its high strength and toughness as grain coarsening begins. Nevertheless, the steel maintains an optimal balance between ductility and strength, rendering it suitable for applications that require moderate heat resistance.

At temperatures exceeding 600 °C and reaching 750 °C, the microstructure undergoes substantial alterations. Images 6 (e), 6 (g) and 6 (p), taken at 600 °C, portray a notable increase in grain coarsening as exposure time is extended from 30 to 150 min. While the microstructure remains relatively stable at 600 °C, it undergoes a more pronounced alteration at 750 °C. The microstructural examination at 750°C, as depicted in images 7 (d), 7 (f), 6 (j), 6 (l), evinces a considerable increase in grain size, with the emergence of extensive regions of ferrite and pearlite. This extensive grain coarsening results in a marked reduction in both tensile and yield strengths, which leads to increased softness and ductility in the steel. Prolonged exposure to elevated temperatures serves to exacerbate microstructural changes, resulting in the most significant grain growth within a period of 120 to 150 min. The formation of coarse grains under these conditions renders the steel unsuitable for applications requiring high strength and durability, as it becomes more susceptible to deformation and less resistant to mechanical stresses. In conclusion, the evolution of the microstructure of hot-rolled steel under varying thermal treatments demonstrates the significant impact of both temperature and exposure time on the material's structural changes. Lower temperature conditions and shorter exposure durations effectively preserve fine grains and maintain superior mechanical properties, whereas higher temperatures and extended exposure result in significant grain coarsening and a concomitant reduction in strength. It is imperative to gain a comprehensive understanding of these changes in order to optimize the thermal processing of hot-rolled steel and meet specific requirements in industrial applications.

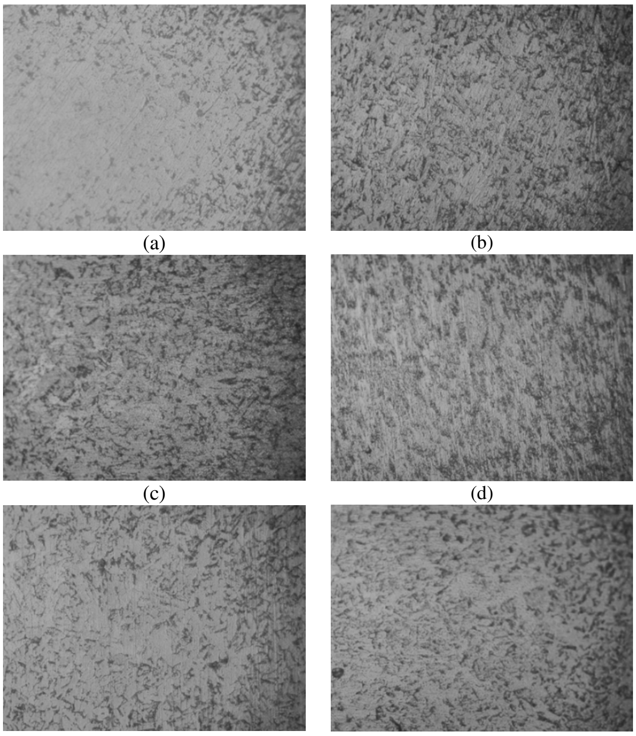

(a) (b)
(c) (d)
(e) (f)

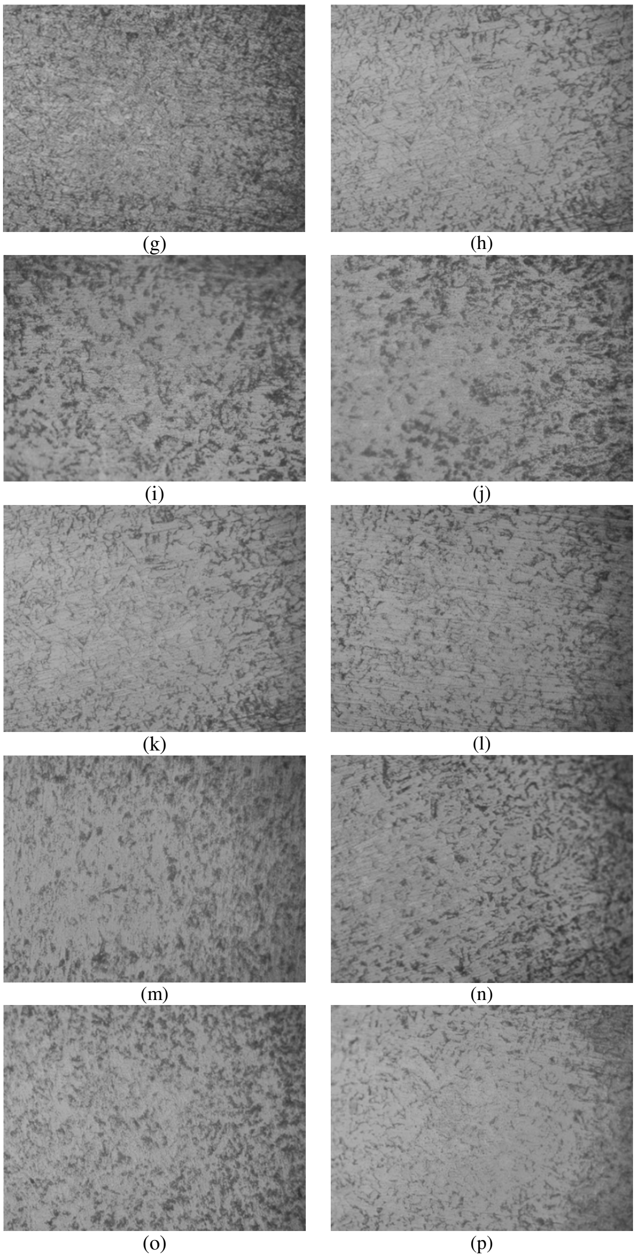

Fig. 6. Microstructures for experiments (B-Q) with temperature and time: (a) 600 C° and 30 min, (b) 300 C° and 90 min, (c) 600 C° and 150 min, (d) 150 C° and 60 min, (e) 600 C° and 120 min, (f) 150 C° and 90 min, (g) 300 C° and 120 min, (h) 300 C° and 60 min, (i) 750 C° and 150 min, (j) 750 C° and 90 min, (k) 300 C° and 30 min, (l) 750 C° and 60 min, (m) 450 C°and 90 min, (n) 450 C° and 60 min, (o) 300 C° and 150 min, (p) 600 C° and 60 min.

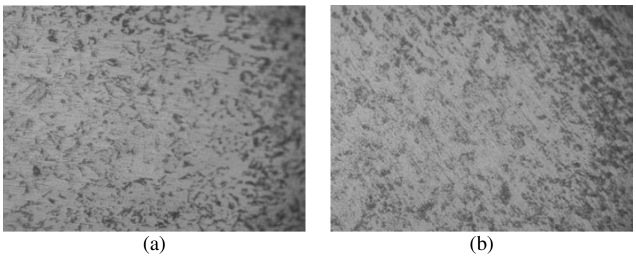

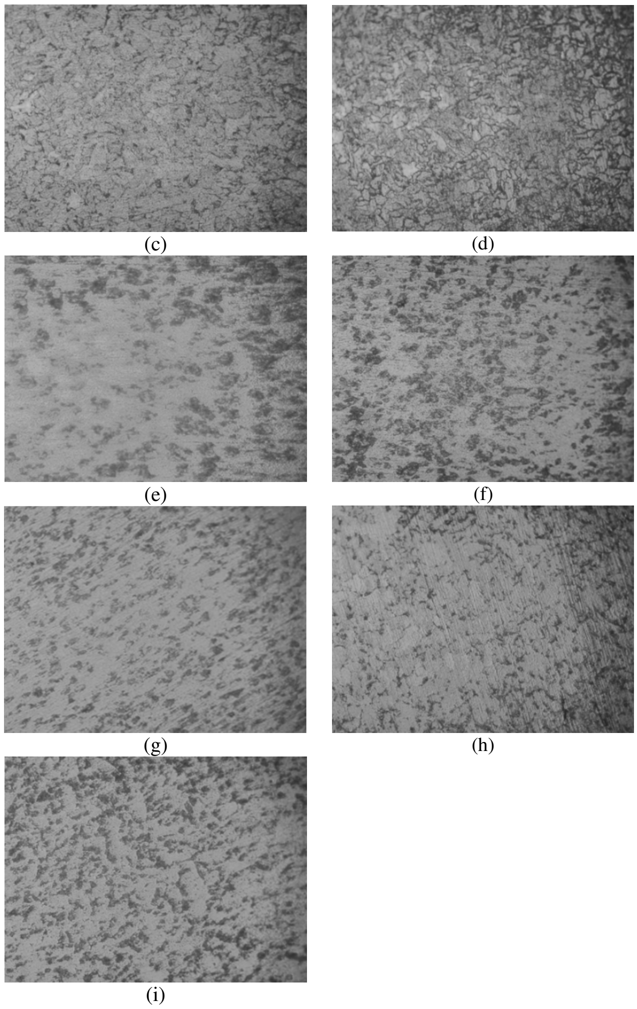

Fig. 7. Microstructures for experiments (R-Z) with temperature and time: (a) 150 C° and 120 min, (b) 450 C° and 120 min, (c) 450 C° and 150 min, (d) 750 C° and 120 min, (e) 450 C° and 30 min, (f) 750 C° and 30 min, (g) 600 C° and 90 min, (h) 150 C° and 30 min, (i) 150 C° and 150 min.

IV. MODEL DEVELOPMENT

The objective of the model development was to create predictive models for each criterion variable—yield strength, tensile strength, and elongation—based on the predictor variables of temperature and time. The Minitab V20 software was employed for statistical analysis, including stepwise regression, in order to identify the optimal models. The correlation matrix, as shown in Figure 8, offered valuable insights into the relationships between predictor and criterion variables, thereby aiding the selection of the most appropriate model. The correlation matrix indicated that temperature demonstrated robust positive correlations with both tensile strength (0.92) and yield strength (0.70), thereby suggesting that temperature is a substantial predictor of these mechanical properties. However, the correlation between temperature and elongation was moderate (0.63), indicating that while temperature influences elongation, its effect is not as pronounced. In contrast, time demonstrated a markedly robust correlation with tensile strength (0.92), underscoring the pivotal role of soaking time in enhancing tensile strength. However, its impact on yield strength (0.26) and elongation (0.34) was comparatively less pronounced. These correlations were instrumental in the selection of predictor variables for model development, ensuring that the variables with the strongest relationships were given particular emphasis. For yield strength, several models were tested, as presented in Table VII, beginning with a linear model, which yielded an R^2 of 88%. As nonlinear relationships were explored, the power model below provided the best fit, with an R^2 of 97.6%:

$$Y = 19.0039 \cdot \mathrm{Temp}^{0.333} + 28.9566 \cdot \mathrm{Time}^{0.333} \quad (1)$$

This model was selected on the basis of its high explanatory power, which accounts for 97.6% of the variance in yield strength. The standard error of the regression (S) for this model was 41.3720, indicating that the model exhibits a reasonable level of precision in predicting yield strength.

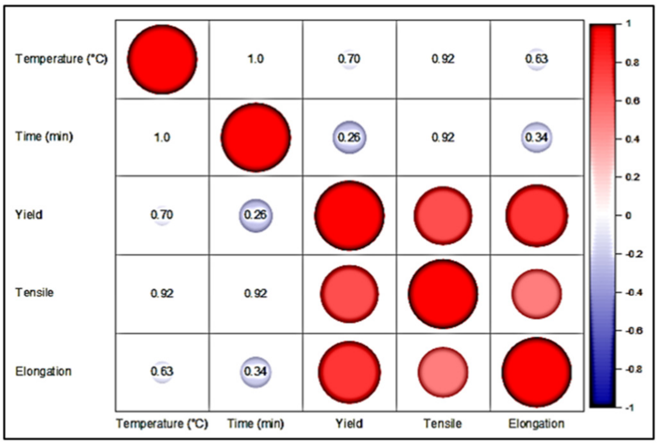

Fig. 8. Correlation matrix for the criterion and predictor variables.

TABLE VIII. GENERAL MODEL STRUCTURES FOR REH

	Criterion	Model Structure	Type	R^2 (%)
1	Yield	$Y= a + b\,x_1 + c\,x_2$	Linear	88
2	Yield	$Y= a + b\,x_1 + c\,x_2^{0.5}$	Power	93.7
3	Yield	$Y= a + b\,x_1^{0.5} + c\,x_2$	Power	93.9
4	Yield	$Y= a + b\,x_1 + c\,x_2^{0.3}$	Power	97
5	Yield	$Y= a + b\,x_1^{0.3} + c\,x_2$	Power	96.5
6	Yield	$Y= a + b\,x_1^{0.3} + c\,x_2^{0.5}$	Power	97
7	Yield	$Y= a + b\,x_1^{0.5} + c\,x_2^{0.3}$	Power	97
8	Yield	$Y= a + b\,x_1^{0.3} + c\,x_2^{0.3}$	Power	97.6

TABLE IX. GENERAL MODEL STRUCTURES FOR RM

	Criterion	Model Structure	Type	R^2 (%)
1	Tensile	$Y= a + b\,x_1 + c\,x_2$	Linear	89
2	Tensile	$Y= a + b\,x_1 + c\,x_2^{0.5}$	Power	94.6
3	Tensile	$Y= a + b\,x_1^{0.5} + c\,x_2$	Power	94.6
4	Tensile	$Y= a + b\,x_1 + c\,x_2^{0.3}$	Power	97
5	Tensile	$Y= a + b\,x_1^{0.3} + c\,x_2$	Power	97
6	Tensile	$Y= a + b\,x_1^{0.3} + c\,x_2^{0.5}$	Power	97.6
7	Tensile	$Y= a + b\,x_1^{0.5} + c\,x_2^{0.3}$	Power	97.6
8	Tensile	$Y= a + b\,x_1^{0.3} + c\,x_2^{0.3}$	Power	98.2

With regard to the ultimate tensile strength, the linear model initially yielded an R^2 of 89%, as illustrated in Table IX. Nevertheless, the power model demonstrated superior performance, with an R^2 of 98.2%:

$$Y = 44.2650 \cdot \mathrm{Temp}^{0.333} + 25.6634 \cdot \mathrm{Time}^{0.333} \quad (2)$$

The standard error of the regression (S) for this model was 52.1638, indicating a slight increase in variability in the prediction of tensile strength compared to the yield strength model. However, this remains within an acceptable range for accurate prediction. Regarding the variable of elongation, the linear model yielded an R^2 of 88%, as shown in Table X. However, subsequent analysis indicated that the power model, was the most accurate, with an R^2 of 97.9%:

$$Y = 3.89961 \cdot \mathrm{Temp}^{0.333} + 2.37505 \cdot \mathrm{Time}^{0.333} \quad (3)$$

The standard error of the regression (S) for this model was 4.99668, displaying the lowest variability among the models, indicating high precision in predicting elongation.

TABLE X. GENERAL MODEL STRUCTURES FOR ELONGATION

	Criterion	Model Structure	Type	R^2 (%)
1	Elongation	$Y= a + b\,x_1 + c\,x_2$	Linear	88
2	Elongation	$Y= a + b\,x_1 + c\,x_2^{0.5}$	Power	93.8
3	Elongation	$Y= a + b\,x_1^{0.5} + c\,x_2$	Power	94
4	Elongation	$Y= a + b\,x_1 + c\,x_2^{0.3}$	Power	96.4
5	Elongation	$Y= a + b\,x_1^{0.3} + c\,x_2$	Power	96.6
6	Elongation	$Y= a + b\,x_1^{0.3} + c\,x_2^{0.5}$	Power	97.2
7	Elongation	$Y= a + b\,x_1^{0.5} + c\,x_2^{0.3}$	Power	97.3
8	Elongation	$Y= a + b\,x_1^{0.3} + c\,x_2^{0.3}$	Power	97.9

The variables a, b, and c are constants, while x_1 is the temperature in (°C) and x_2 is time in min. In conclusion, the power models exhibited consistently superior predictive accuracy for all criterion variables, with R^2 values exceeding 97%. These models are therefore the most effective at capturing the relationships between temperature, time, and the mechanical properties of hot-rolled steel. In light of these findings, it can be concluded that the power models developed in this study are reliable predictors of yield strength, tensile strength, and elongation. These models offer valuable insights for optimizing process parameters in industrial applications.

V. OPTIMIZATION TECHNIQUE

An empirical model was developed for the response parameters, which included yield strength (*Reh*), tensile strength (*Rm*), and elongation (*E*), using the design of experiments technique. This was done by considering all possible combinations of the 25 experiments. The desirability function method, initially proposed in [30], is an effective approach for addressing multi-optimization challenges. This method was employed to ascertain the optimal operational conditions that yield the most desirable response values [31, 32]. A multi-response optimization problem can be formally expressed as:

$$\text{Optimize } [y_1(x), y_2(x), \ldots, y_n(x)] \text{ subject to } x \in \Omega \quad (4)$$

where x is the vector of input variables, Ω is the experimental region of x, and $y_i(x)$ is the fitting response function of the i_{th} response variable y_j, where i = 1, 2, …, m, and m is the number of responses [33]. The experimental results were converted into a single response on a (0, 1) scale by calculating their desirability (d), where 0 represents the lowest desirable value and 1 the highest [34]. The maximum desirability values were recorded as the optimal combination of parameters. The scale of the response parameters was divided according to the function: Nominal the Better (NTB), Smaller the Better (STB), and Larger the Better (LTB). The choice of scale depends on the application areas, which are explained individually [35]:

$$d_i(Y)_i = \begin{cases} 0 & Y < L \\ \left(\frac{Y-L}{T-L}\right)^r & L \le Y \le T \\ 1 & Y > T \end{cases} \quad (5)$$

$$d_i(Y)_i = \begin{cases} 0 & Y < T \\ \left(\frac{U-Y}{U-T}\right)^r & T \le Y \le U \\ 1 & Y > U \end{cases} \quad (6)$$

$$d_i(Y_i) = \begin{cases} 0 & Y < L \\ \left(\frac{Y-L}{T-L}\right)^{r_1} & L \le Y \le T \\ \left(\frac{U-Y}{U-T}\right)^{r_2} & T \le Y \le U \\ 0 & Y > U \end{cases} \quad (7)$$

where Y is the response parameter, U is the upper limit, L is the lower limit, T is the target value, and r, r_1, and r_2 are the weights. The overall desirability function of explanation of multiple responses is defined as:

$$D = (d_1 \times d_2 \times d_3 \times \ldots d_n) = \left(\prod_{i=1}^{n} d_i\right)^{1/n} \quad (8)$$

where D is the composite desirability, d_1, d_2, d_3, ..., d_n are the desirability values for different responses, and n is the number of responses. The individual desirability values corresponding to each parameter were calculated based on (5), as listed in Table XI. Equation (5) defines LTB, where the response value is expected to be larger than the lower bound, whereas (6) defines STB, where the estimated response value is expected to be smaller than the upper bound, and (7) defines NTB, where the response is expected to reach a specific target value [36].

TABLE XI. EXPERIMENT AND MEASURED RESPONSE PARAMETERS (INDIVIDUAL DESIRABILITY INDEX)

Exp.No.	Individual desirability index		
	Yield strength (MPa), *Reh*	Tensile strebgth (MPa), *Rm*	Elongation (%)
B	0.87	0.69	0.53
C	0.79	1.00	0.67
D	0.81	0.95	0.42
E	0.40	0.67	0.37
F	0.17	0.66	0.15
G	0.98	0.87	1.00
H	1.00	0.82	0.97
I	0.77	0.74	0.60
J	0.74	0.66	0.58
K	0.13	0.74	0.31
L	0.87	0.75	0.86
M	0.66	0.79	0.86
N	0.58	0.72	0.83
O	0.51	0.51	0.67
P	0.11	0.44	0.42
Q	0.62	0.38	0.67
R	0.53	0.57	0.78
S	0.49	0.33	0.69
T	0.40	0.39	0.58
U	0.09	0.31	0.18
V	0.47	0.39	0.40
W	0.49	0.26	0.67
X	0.25	0.11	0.41
Y	0.21	0.05	0.23
Z	0.00	0.00	0.00

The initial stage of the investigation entailed an examination of the outcomes yielded by the response parameters, with the objective of elucidating the interrelationship between the process and the response parameters. The subsequent phase comprised a discourse on the data obtained from the full factorial design, which was conducted with the aid of Minitab 20 software and a comprehensive quadratic response surface model:

$$Y = \beta_0 + \sum_{i=1}^{k} \beta_1 x_i + \sum_{i=1}^{k} \beta x_i x_i + \sum_{i<j} \sum \beta_{ij}\, x_i\, x_j \quad (9)$$

where y is the response, x_i is the i_{th} factor, and k is the total number of factors.

(a)

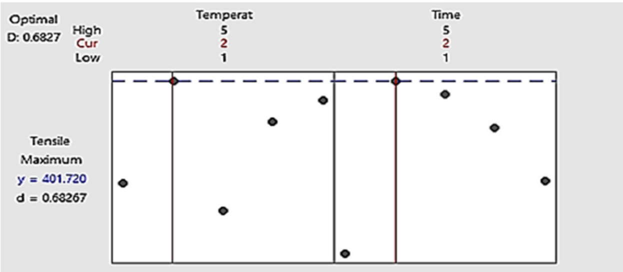

(b)

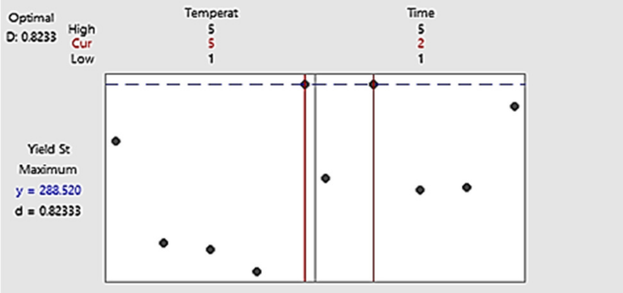

(c)

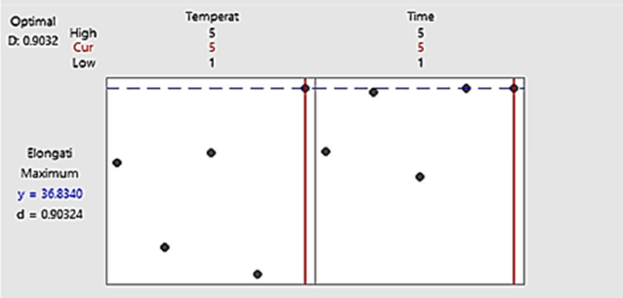

Fig. 9. The optimized process parameters for individually maximizing desirability function: (a) represents the ultimate tensile strength, (b) Yield strength and (c) elongation.

A regression analysis was conducted using Minitab 20 to ascertain the optimal fit between the response function and the experimental data. The final regression equations for elongation, tensile strength, and yield strength, incorporating all coefficients, are:

$$Elongation\ (\%) = 34.810 + 0.362(Temp1) - 0.996(Temp2) + 0.518(Temp3) - 1.418(Temp4) +$$

$1.534(Temp5)\ -0.498(Time1)\ +0.436(Time2)\ -$
$0.912(Time3)\ +0.484(Time4)\ +0.490(Time5)$ (10)

$Rm\ =\ 392.48-3.28(Temp1)\ +4.32(Temp2)\ -$
$5.28(Temp3)\ +1.32(Temp4)\ +2.92(Temp5)\ -$
$7.88(Time1)\ +4.92(Time2)\ +3.92(Time3)\ +$
$1.52(Time4)\ -2.48(Time5)$ (11)

$Reh\ =\ 272.28\ +5.12(Temp1)\ -4.08(Temp2)\ -$
$4.68(Temp3)\ -6.68(Temp4)\ +10.32(Temp5)\ -$
$2.68(Time1)\ +5.92(Time2)\ -3.68(Time3)\ -$
$3.48(Time4)\ +3.92(Time5)$ (12)

The desirability function maximized the response parameters, as shown in Figure 9.

Figure 10 displays the optimization of multi-process parameters for hot rolled steel with an optimum response parameter. The optimal process parameter levels were identified as those that maximized the desirability function, as calculated for the respective responses and presented in Table XII. The response parameter was of equal importance. Table XIII shows the combined desirability function for each response parameter, which was optimized simultaneously with the optimal factor levels.

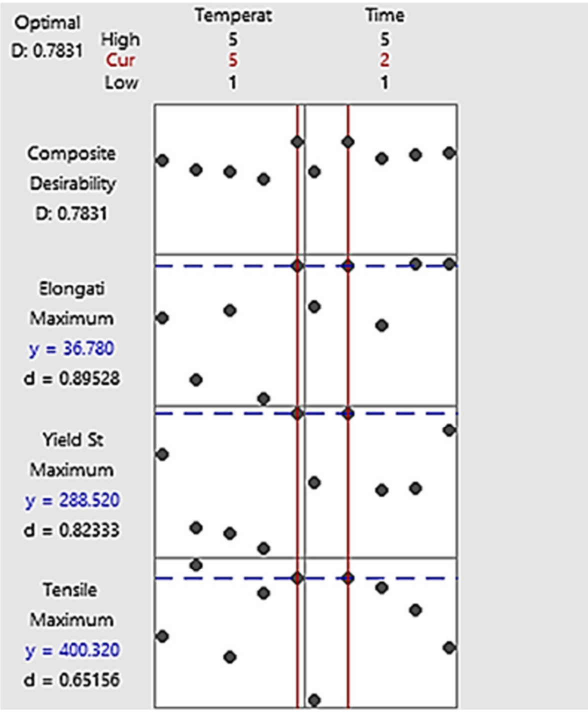

Fig. 10. Multi-response parameters for hot rolled steel sections.

TABLE XII. OPTIMUM RESPONSE WITH LEVELS AND TARGET RESPONSE

Response	Goal	Lower	Target	Weight	Importance
Rm (MPa)	Max.	371.00	416.00	1	1
Elongation (%)	Max.	30.71	37.49	1	1
Reh (MPa)	Max.	249.00	297.00	1	1

TABLE XIII. OPTIMUM FACTOR LEVELS AND PREDICTED RESPONSE FOR INDIVIDUAL AND COMBINED RESPONSE

Optimum factor levels and predicted response for individual response					**Optimum response levels and predicted response for combined strength**
Temp (° C)	Time (min.)	*Rm* (MPa) Fit	Elongation (%) Fit	*Reh* (MPa) Fit	Composite Desirability
5	2	400.32	36.78	288.52	0.783121

The Analysis of Variance (ANOVA) method was employed to validate the full factorial design analysis results of the experiments, as it produces statistically reliable results. This process was undertaken to estimate the percentage contribution of each response parameter of the heat-treated samples. As manifested in Table XIV, the highest percentage of time was identified as the primary process parameter influencing the responses associated with elevated temperatures, such as those observed in the combustion of hot rolled steel. This parameter demonstrated a contribution of 62%.

TABLE XIV. ANOVA RESULTS

Source	DF	SS	MS	Contribution (%)
Temperature (°C)	4	337.8	84.46	38%
Time (min.)	4	550.6	137.66	62%
Error	16	2,725.8	170.36	
Total	24	3,614.2		

In statistical analysis, the Degree of Freedom (DF) is the number of independent variables in a model, the Sum of Squares error (SS) is the sum of the squares of the differences between the observed and predicted values, and the Mean Squares error (MS) is the mean of the squares of the differences between the observed and predicted values.

VI. CONCLUSIONS

This research contributes to the understanding of how hot-rolled steel behaves under fire conditions, in line with today's need for improved material performance in construction. By determining the temperature-dependent mechanical behavior of steel, this work contributes to the refinement of design standards and codes in structural engineering practice. The optimization of response parameters, including ultimate tensile strength, yield strength, and elongation, under the effect of elevated temperatures on hot-rolled steel using a full factorial design-based desirability function can be summarized as:

- Soaking time has been identified as the most important factor influencing the mechanical properties of hot-rolled steel, accounting for 62% of the observed variation. Prolonged soaking at elevated temperatures results in significant grain coarsening, which negatively affects tensile strength, yield strength, and ductility.
- Higher temperatures, especially above 600 °C, have a significant effect on microstructural changes, causing pronounced grain coarsening. This coarsening results in a reduction in tensile strength and yield strength, producing a softer, more ductile material that is less resistant to mechanical stress.

- The study showed that the optimum process conditions for hot-rolled steel are characterized by a temperature of 650 °C and a soaking time of 60 min. These specific parameters resulted in the maximum values of mechanical properties, namely: an ultimate tensile strength of 400.2 MPa, a yield strength of 288.52 MPa, and an elongation of 36.78%. this result indicates an optional balance between strength and ductility.
- This study highlights the need for careful control of temperature and soaking time in industrial processes. An effective management of these parameters is essential to improve the mechanical properties of hot-rolled steel, particularly in applications subject to significant thermal stress.

Future research projects should prioritize the exploration of the behavior of hot-rolled steel across an extended temperature spectrum, particularly at temperatures exceeding 750 °C. An investigation of the performance of steel under such extreme conditions—especially those analogous to scenarios encountered in building fires—will yield valuable insights into the material's limits regarding performance and ductility when subjected to severe thermal stresses. Furthermore, it is essential to initiate long-term exposure studies that simulate real-world conditions, such as prolonged fire incidents, in order to gain a comprehensive understanding of the alterations in steel properties over extended durations. These empirical data are crucial for the formulation of accurate predictive models that inform structural safety assessments in the context of fire exposure.

REFERENCES

[1] A. Grajcar, A. Kozłowska, S. Topolska, and M. Morawiec, "Effect of Deformation Temperature on Microstructure Evolution and Mechanical Properties of Low-Carbon High-Mn Steel," *Advances in Materials Science and Engineering*, vol. 2018, no. 1, 2018, Art. no. 7369827, https://doi.org/10.1155/2018/7369827.

[2] A. Kozłowska and A. Grajcar, "Effect of Elevated Deformation Temperatures on Microstructural and Tensile Behavior of Si-Al Alloyed TRIP-Aided Steel," *Materials*, vol. 13, no. 22, Jan. 2020, Art. no. 5284, https://doi.org/10.3390/ma13225284.

[3] M. Htun, S. Kyaw, and K. Lwin, "Effect of Heat Treatment on Microstructures and Mechanical Properties of Spring Steel," *Journals of Metals, Materials and Minerals*, vol. 18, no. 2, pp. 191–197, Jan. 2008.

[4] J. Chen, B. Young, and B. Uy, "Behavior of High Strength Structural Steel at Elevated Temperatures," *Journal of Structural Engineering*, vol. 132, no. 12, pp. 1948–1954, Dec. 2006, https://doi.org/10.1061/(ASCE)0733-9445(2006)132:12(1948).

[5] I. Litovchenko *et al.*, "The Microstructure and Mechanical Properties of Ferritic-Martensitic Steel EP-823 after High-Temperature Thermomechanical Treatment," *Metals*, vol. 12, no. 1, Jan. 2022, Art. no. 79, https://doi.org/10.3390/met12010079.

[6] M. H. Al-Sherrawi, A. M. Saadoon, S. Sotnik, and V. Lyashenko, "Information model of plastic products formation process duration by injection molding method," *International Journal of Mechanical Engineering and Technology*, vol. 9, no. 3, pp. 357–366, Mar. 2018.

[7] L. He, H. Li, and C. Wang, "Effect of Austenitization Temperature on Microstructure and Mechanical Properties of B1500HS Boron Steel in the Hot Stamping," *MATEC Web of Conferences*, vol. 67, 2016, Art. no. 03001, https://doi.org/10.1051/matecconf/20166703001.

[8] Z. Hou, D. Wu, S. Zheng, X. Yang, Z. Li, and Y. Xu, "Effect of Holding Temperature on Microstructure and Mechanical Properties of High-Strength Multiphase Steel," *Steel Research International*, vol. 87, no. 9, pp. 1203–1212, Dec. 2015, https://doi.org/10.1002/srin.201500331.

[9] S. H. Abro, A. Chandio, A. R. Jamali, and S. A. Shah, "Influence of Austenite Phase Transformation on Existing Microstructure of Low C-Mn Steel," *Engineering, Technology & Applied Science Research*, vol. 8, no. 6, pp. 3525–3529, Dec. 2018, https://doi.org/10.48084/etasr.2324.

[10] L. Čížek *et al.*, "Mechanical properties of magnesium alloy AZ91 at elevated temperatures," *Journal of Achievements in Materials and Manufacturing Engineering*, vol. 18, no. 1–2, pp. 203–206, Aug. 2006.

[11] R. Song, D. Ponge, D. Raabe, J. G. Speer, and D. K. Matlock, "Overview of processing, microstructure and mechanical properties of ultrafine grained bcc steels," *Materials Science and Engineering: A*, vol. 441, no. 1, pp. 1–17, Dec. 2006, https://doi.org/10.1016/j.msea.2006.08.095.

[12] J. Outinen, Mechanical properties of structural steels at high temperatures and after cooling down. Helsinki, Finland: Helsinki University of Technology, 2007.

[13] G. Hu, M. A. Morovat, J. Lee, E. Schell, and M. Engelhardt, "Elevated Temperature Properties of ASTM A992 Steel," *Structures Congress 2009: Don't Mess with Structural Engineers: Expanding Our Role*, pp. 1–10, Apr. 2012, https://doi.org/10.1061/41031(341)118.

[14] L. Čížek *et al.*, "Structure and mechanical properties of Mg-Si alloys at elevated temperatures," *Journal of Achievements in Materials and Manufacturing Engineering*, vol. 35, no. 1, pp. 37–46, Jul. 2009.

[15] A. Magee, "Mechanical properties and microstructural characteristics of an Al-Mg alloy with bimodal grain size at room and elevated temperatures," MSc Thesis, University of Alabama Libraries, Tuscaloosa, AL, USA, 2012.

[16] L. Milović, T. Vuherer, I. Blačić, M. Vrhovac, and M. Stanković, "Microstructures and mechanical properties of creep resistant steel for application at elevated temperatures," *Materials & Design*, vol. 46, pp. 660–667, Apr. 2013, https://doi.org/10.1016/j.matdes.2012.10.057.

[17] A. Bhowmik *et al.*, "Microstructure and mechanical properties of Cr–Ta–Si Laves phase-based alloys at elevated temperatures," *Philosophical Magazine*, vol. 94, no. 34, pp. 3914–3944, Dec. 2014, https://doi.org/10.1080/14786435.2014.971086.

[18] A. Zieliński, M. Sroka, A. Hernas, and M. Kremzer, "The Effect of Long-Term Impact of Elevated Temperature on Changes in Microstructure and Mechanical Properties of HR3C Steel," *Archives of Metallurgy and Materials*, vol. 61, no. 2A, pp. 761–766, 2016, https://doi.org/10.1515/amm-2016-0129.

[19] J. Jaworski and T. Trzepieciński, "Properties of low-alloy high-speed steel at elevated temperature," *Metalurgija*, vol. 56, no. 1–2, pp. 75–78, Jan. 2017.

[20] Y. Tian, H. Wang, Y. Li, Z. Wang, and G.-D. Wang, "The Analysis of the Microstructure and Mechanical Properties of Low Carbon Microalloyed Steels after Ultra Fast Cooling," *Materials Research*, vol. 20, no. 3, pp. 853–859, Jun. 2017, https://doi.org/10.1590/1980-5373-mr-2016-0627.

[21] A. Hussein, L. Abbas, and W. Hasan, "Optimization of Heat Treatment Parameters for the Tensile Properties of Medium Carbon Steel," *Engineering and Technology Journal*, vol. 36, pp. 1091–1099, Oct. 2018, https://doi.org/10.30684/etj.36.10A.10.

[22] J. Ren, Q. Chen, J. Chen, and Z. Liu, "Role of vanadium additions on tensile and cryogenic-temperature charpy impact properties in hot-rolled high-Mn austenitic steels," *Materials Science and Engineering: A*, vol. 811, Apr. 2021, Art. no. 141063, https://doi.org/10.1016/j.msea.2021.141063.

[23] V. S. Sam *et al.*, "Influence of elevated temperature on buckling capacity of mild steel-based cold-formed steel column sections– experimental investigation and finite element modelling," *Journal of Structural Fire Engineering*, vol. 15, no. 3, pp. 314–337, Nov. 2023, https://doi.org/10.1108/JSFE-08-2023-0033.

[24] B. Jiang, Y. Qu, M. Wang, G. Lou, and G. Li, "Mechanical properties of Q355 hot-rolled steel during the entire fire process," *Journal of Constructional Steel Research*, vol. 215, Apr. 2024, Art. no. 108565, https://doi.org/10.1016/j.jcsr.2024.108565.

[25] L. Gupta, N. Keskar, B. C. Maji, R. N. Singh, and M. Krishnan, "Effect of Heat Treatments on the Microstructure and Mechanical Properties of SS317L/ASTM SA516 GR60 Steel Clad Plate Fabricated Through Hot

Roll Bonding," *Metallurgical and Materials Transactions A*, vol. 55, no. 11, pp. 4354–4372, Nov. 2024, https://doi.org/10.1007/s11661-024-07547-w.

[26] F. Tariq, "Combined effects of corrosion and fire on load-carrying response of hot-rolled steel reinforcement," *Journal of Structural Fire Engineering*, vol. 15, no. 4, pp. 619–644, Jul. 2024, https://doi.org/10.1108/JSFE-09-2023-0034.

[27] *ISO 4995:2014 Hot-rolled steel sheet of structural quality*. International Standard Organization, 2014.

[28] A. Al-Mosawe, H. Agha, L. Al-Hadeethi, and R. Al-Mahaidi, "Efficiency of image correlation photogrammetry technique in measuring strain," *Australian Journal of Structural Engineering*, vol. 19, no. 3, pp. 207–213, Jul. 2018, https://doi.org/10.1080/13287982.2018.1480304.

[29] M. I. Mohamed, "Studies of the Properties and Microstructure of Heat Treated 0.27% C and 0.84% Mn Steel," *Engineering, Technology & Applied Science Research*, vol. 8, no. 5, pp. 3484–3487, Oct. 2018, https://doi.org/10.48084/etasr.2065.

[30] D. Fuller and W. Scherer, "The desirability function: underlying assumptions and application implications," in *SMC'98 Conference Proceedings. 1998 IEEE International Conference on Systems, Man, and Cybernetics*, San Diego, CA, USA, Oct. 1998, vol. 4, pp. 4016–4021 vol.4, https://doi.org/10.1109/ICSMC.1998.726717.

[31] A. A. Alfahad and A. M. Burhan, "BIM-Supporting System by Integrating Risk Management and Value Management," *Engineering, Technology & Applied Science Research*, vol. 13, no. 6, pp. 12130–12137, Dec. 2023, https://doi.org/10.48084/etasr.6427.

[32] E. M. Mahmood, A. A. Allawi, and A. El-Zohairy, "Analysis and Residual Behavior of Encased Pultruded GFRP I-Beam under Fire Loading," *Sustainability*, vol. 14, no. 20, Jan. 2022, Art. no. 13337, https://doi.org/10.3390/su142013337.

[33] D.-H. Lee, I.-J. Jeong, and K.-J. Kim, "A desirability function method for optimizing mean and variability of multiple responses using a posterior preference articulation approach," *Quality and Reliability Engineering International*, vol. 34, no. 3, pp. 360–376, 2018, https://doi.org/10.1002/qre.2258.

[34] N. Barka *et al.*, "Full factorial experimental design applied to oxalic acid photocatalytic degradation in TiO2 aqueous suspension," *Arabian Journal of Chemistry*, vol. 7, no. 5, pp. 752–757, Nov. 2014, https://doi.org/10.1016/j.arabjc.2010.12.015.

[35] I. Y. Enis, H. Sezgin, and T. G. Sadikoglu, "Full factorial experimental design for mechanical properties of electrospun vascular grafts," *Journal of Industrial Textiles*, vol. 47, no. 6, pp. 1378–1391, Feb. 2018, https://doi.org/10.1177/1528083717690614.

[36] B. John, "Application of desirability function for optimizing the performance characteristics of carbonitrided bushes," *International Journal of Industrial Engineering Computations*, vol. 4, no. 3, pp. 305–314, 2013.